A NOVEL APPROACH FOR PREDICTING BIREFRINGENCE OF OPTICAL PARTS

Yuan-Rong Chang[1], Hsien-Sen Chiu[1], Wen-Hsien Yang[1], and Rong-Yeu Chang [2]

1. CoreTech System Co., Ltd., Hsinchu, Taiwan

2. Dept. of Chemical Engineering, National Tsing-Hua University, HsinChu, Taiwan

Abstract

Plastic optical parts or components have been used in many industrial applications, such as optical disks, lenses, and waveguides. For the development of optical products, the control of birefringence is crucial. Basically, it is dependent on optical characteristics of material and global features given by polymer processing. However, the prediction and control of birefringence is difficult. In this study, a novel approach for the prediction of birefringence distribution of injection-molded parts is developed by the 3D simulation technology, which incorporates photoelastic analysis and viscoelastic mechanics.

Introduction

With the growth of plastics industry, more and more injection-molded parts such as optical disks, lenses, and waveguides, are widely used in optical applications for their good optical performance. For the development of optical parts, the birefringence introduced by molecular orientations during injection molding, which leads to optical anisotropy, is one of the most important controls. Birefringence, or double refraction, is referred to the decomposition of a ray of light into two rays when it passes through transparent materials. When polarized light passes through these materials, light and shade fringes appear, whose magnitudes are related to the difference in principal stresses.

The birefringence in optical parts is primarily caused by two reasons. One is the flow-induced residual stress attributed to molecular orientation during filling. The other is the thermal residual stress due to an inequilibrium contraction during cooling[1]. The flow-induced residual stress is generated by the high shear rate of plastics flow during filling, and can be relaxed or frozen during post-filling processes and after ejection, while the thermal-induced residual stress is created by the inequilibrium density or the shrinkage of plastic materials cooled below the glass transition temperature, T_g [2].

The flow-induced stress is generally considered smaller than the thermal-induced stress. However, it is not possible to neglect the former, especially in thin-wall molding, for the frozen-in orientation of polymer molecules affects the mechanical anisotropy, thermal and optical properties, and the long-term dimensional stability. Frozen layers on the surface of mold cavities act as poor thermal conductors. Molecular orientations in the hot core are allowed to relax. Yet the whole parts are cooled and frozen in a very short period and thus molecular orientations are not completely relaxed in thin-wall molding. Therefore, the flow-induced stress is significant for thin-wall parts, while the thermal-induced stress dominates the birefringence phenomena in thick-wall parts.

To get better control of birefringence, various methods have been proposed and developed to investigate the birefringence phenomena both numerically and experimentally [3-8]. In numerical approaches, the conventional 2.5D simulation can not deliver a promising birefringence prediction due to the inherent assumption and model simplification through the middle plane construction. Consquently, a true 3D numerical approach is in great demand for these circumstances.

In this study, a new approach is used to predict the birefringence for injection parts, which is developed by integrating a true 3D numerical analysis and the viscoelastic model for polymer materials in injection molding simulations. Numerical results of the present model show reasonable agreement with the experimental results reported in the literature.

Numerical Modeling

It is assumed that polymer melts behave as the viscoealstic fluid. Therefore, the non-isothermal 3D flow motion can be mathematically described in the followings:

$$\frac{\partial \rho}{\partial t} + \nabla \cdot \rho \mathbf{u} = 0 , \tag{1}$$

$$\frac{\partial}{\partial t}(\rho \mathbf{u}) + \nabla \cdot (\rho \mathbf{u}\mathbf{u} - \boldsymbol{\sigma}) = \rho \mathbf{g} , \tag{2}$$

$$\boldsymbol{\sigma} = -p\mathbf{I} + \tau , \tag{3}$$

$$\rho C_P \left(\frac{\partial T}{\partial t} + \mathbf{u} \cdot \nabla T \right) = \nabla (\mathbf{k} \nabla T) + \frac{1}{2} \tau : (\nabla \mathbf{u} + \nabla \mathbf{u}^T), \tag{4}$$

where u is the velocity vector, T is the temperature, t is the time, p is the pressure, σ is the total stress tensor, ρ is the density, τ is the extra-stress tensor, k is the thermal conductivity, and C_P is the specific heat. In present work, τ is obtained by the constitutive equation of

Giesekus model:

$$\tau + \lambda \overset{\nabla}{\tau} = -\frac{\alpha\lambda}{\eta_0}\tau\cdot\tau + \eta_0\left(\nabla\mathbf{u} + \nabla\mathbf{u}^T\right), \qquad (5)$$

where λ is the relaxation time, α is the mobility factor, and η_0 is the zero shear viscosity.

A volume fraction function, f, is introduced to track the evolution of the melt front. Here, $f = 0$ is defined as the air phase, $f = 1$ as the polymer melt phase. Hence, the melt front is located within cells with $0 < f < 1$. The advancement of f over time can be expressed as the following transport equation:

$$\frac{\partial f}{\partial t} + \nabla\cdot\left(\mathbf{u}f\right) = 0. \qquad (6)$$

The flow rate or injection pressure is prescribed at mold inlet. The walls of mold are assumed to be non-slip. It is to be noted that only the inlet boundary condition is necessary for the hyperbolic transport equation of volume fraction function.

The collocated cell-centered FVM (Finite Volume Method)-based 3D numerical approach developed in our previous work is applied in this paper [6]. The numerical method is basically a SIMPLE-like FVM with improved numerical stability. Furthermore, the volume-tracking method based on a fixed framework is incorporated in the flow solver to track the evolutions of melt front during molding.

In plastics, the index value varies as a function of the stress applied. This gave rise to the Stress-Optic, or "Brewster's" Law can be expressed as the following:

$$n_1 - n_2 = C_B(\sigma_1 - \sigma_2), \qquad (7)$$

where n_1 and n_2 are the indices of refraction, σ_1 and σ_2 are the principal stresses, and C_B is the Stress-optical constant. This law descried that birefringence is directly proportional to the difference of principal stresses.

The phase difference between the two light vectors traveling through the material at different velocities is known as retardation, δ. The retardation value divided by the thickness of a material, d, and is proportional to the difference between the two indices of refraction, i.e.,

$$\delta = \Delta n d. \qquad (8)$$

The fringe order, N, can be determined by ratio of the retardation value to the wavelength of light, λ, such as the following:

$$\frac{\delta}{\lambda} = N. \qquad (9)$$

Results and discussions

Firstly, the filling of a simple thin-wall plate is studied to validate the proposed approach. The dimension of the plate is 1.8 mm (thickness) x 127 mm (lengh) x 64 (width), as shown in Fig.1. This model is meshed by the hexahedral elements with 14 layers in the thickness direction. Table 1 lists the material, related parameters, and process conditions used in this study. The material used in this study is PS Styron 678U. The melt temperature is 218.3 ℃, mold tmperature is 60 ℃, and filling time is 0.72 seconds. The wavelength is 500 nm. The stress-optical constant is $4.8\cdot10^{-9}\ m^2/N$

Fig.2 (a)-(b) shows numerical results of the distribution of birefringence on the cavity surface and the central cross section of the plate. From these figures, it is observed that birefringence concentrates at the gate end and near the surface of top and bottom walls, for the effect of the flow-induced stress as expected.

Fringed pattern by the present numerical model for the case is plotted in Fig.3. As shown in figure, most of multicolored band or fringed pattern is near the gate and around the surfaces of walls. Compared with the experimental data [7-8], the optical result from the present numerical model shows reasonable consistence with those in the literature.

Furthermore, a sensor point, shown in Fig.4, near the gate is set to detect the variation of birefringence induced by molecular orientation in the thickness direction. A plot of the distribution of birefringence by the present numerical model compared with the experimental data at this point is drawn in Fig.5. As expected, the maximum birefringence occurs near the surface of top wall in proportion to the magnitude of residual stress.

Finally, an industrial lens part is also simulated to further demonstrate the capacity of the proposed approach. The numerical analysis is carried out for a spherical convex lens of which outer radius and thickness are 20 mm and 4.5 mm, as shown in Fig.6. Birefringence is observed from the side views as show in Fig.7 (a)-(b). As shown in figures, birefringence due to the flow-induced residual stress concentrates near the gate. Birefringence near the filling end due to the thermal stress originates from the contraction of geometric curvatures. According to these numerical results, which are consistence with the physical

acknowledgements, it is convinced that the present model

is a promising tool to analyze the behavior of birefringence induced by residue stress during filling.

Conclusions

To get better control of birefringence, various methods have been proposed and developed to investigate the birefringence phenomena both numerically and experimentally [7-8]. In numerical approaches, on one hand, a conventional 2D simulation can not catch birefringence distribution due to the less precision on residual stresses prediction for complex geometrical structures. On the other hand, during the polymer processing such as injection molding, the viscoelastic behavior will affect the birefringence significantly, which makes it difficult to predict. A true 3D numerical approach is in great demand for these circumstances.

In this study, a new approach is employed to predict birefringence for injection parts, which is developed by integrating a true 3D numerical analysis and the viscoelastic model for polymer materials in injection molding simulation. The numerical results show photoelastic or fringed patterns that makes it easier for designers to compare the numerical simulation with the experimental results. The meshing flexibility and the solution capabilities of the proposed approach have made it a highly reliable CAE tool to aid the designer/engineer to analyze and further optimize the micro molding process.

Reference

[1]. Y. B. Lee and T. H. Kwon, *Journal of Materials Processing Technology*, 2001, 111:214-8.
[2]. A. I. Isayev, *Polymer Engineering and Science*, 1983, 23:271-84.
[3]. R. Y. Chang and S.Y. Chiou, *Polymer Engineering and Sscience*, 1995, 35: 1733-47.
[4]. A. I. Leonov, *Rheologica acta*, 1976, 15:.
[5]. M. R. Kamal and V. Tan, *Polymer Engineering and Science*, 1979, 19:.
[6]. R. Y. Chang and W. H. Yang, *International Journal for Numerical Methods in Fluids*, 2001, 37: 125-48.
[7]. K. Park, B. Kim, and D. Yao, *ANTEC proceeding*, 2006:.
[8]. D.C. Angstadt and J. P. Coulter, *ANTEC proceeding*, 2005:.

Acknowledgement

The authors would like to thank the National Science Council of the R.O.C. for partially supporting this research under Contact No. NSC 95-2221-E-007-082.

Key Words

Birefringence, injection molding, 3D, fringed pattern

Tables & Figures

Resin	Filling time	Melt Temp.	Mold Temp.
Ps-Styron 678U	0.72 sec	218.3 ℃	60 ℃
Stress-optical const.		Wavelength of light	
$4.8 \cdot 10^{-9}\ m^2/N$		500 nm	

Table 1. Process conditions of micro-probe part molding experiment

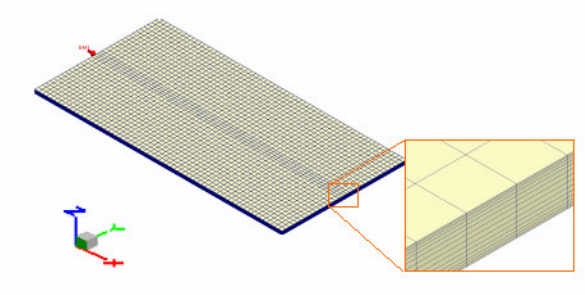

Figure 1 Schematic diagram of the tested rectangular plate.

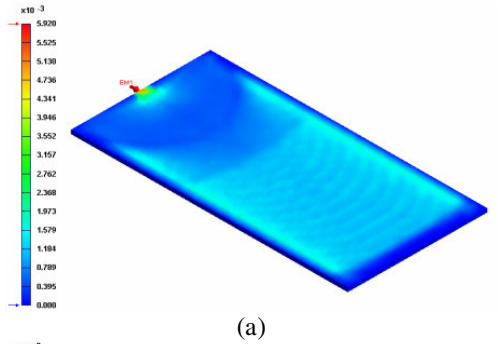

(a)

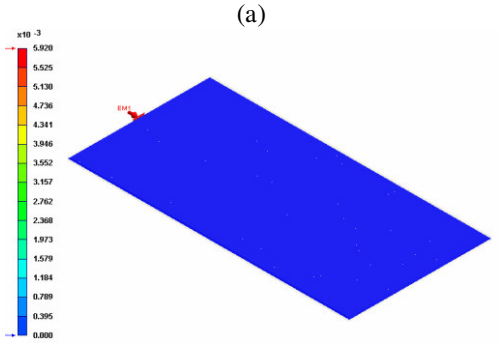

(b)

Figure 2 Numerical results of the distribution of birefringence at (a) the cavity surface, (b) the central, cross section of the plate.

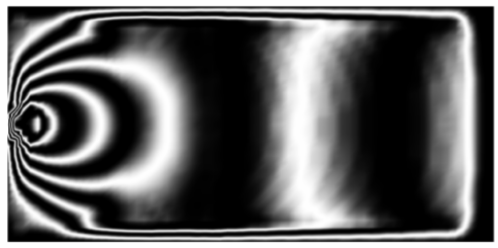

Figure 3 Fringed pattern by the present numerical model.

Figure 4 Schematic diagram of the location of sensor point.

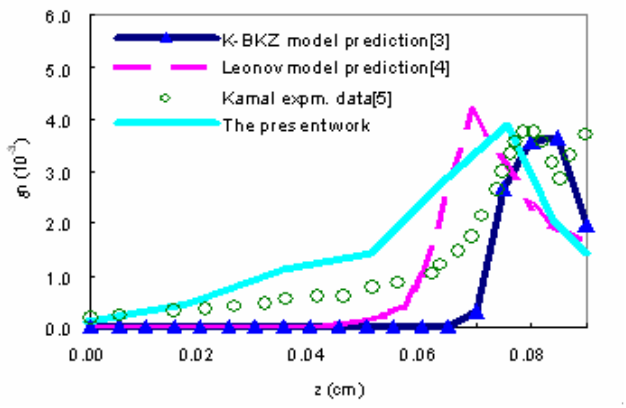

Figure 5 Plots of the distributions of the birefringence along thickness direction at observed point.

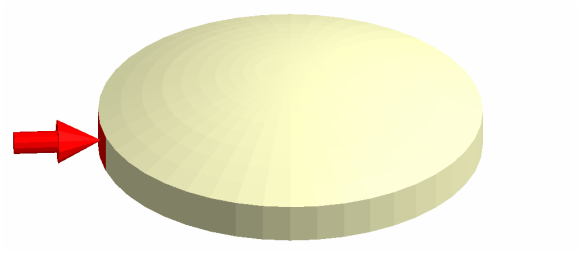

Figure 6 Schematic diagram of the convex lens model.

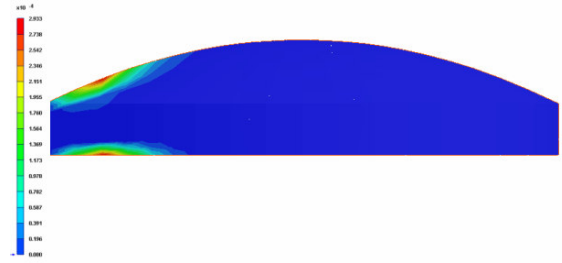

(a)

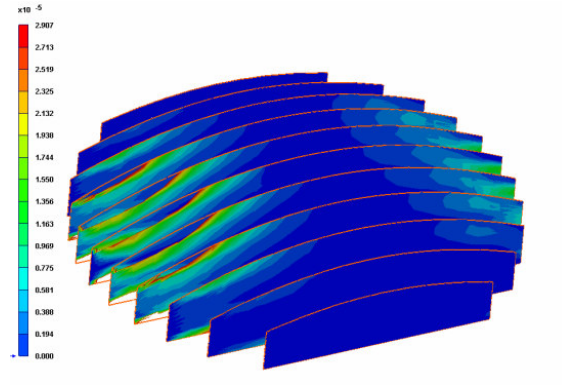

(b)

Figure 7 (a) A side view, (b) sliced side view, of the birefringence distributions of the convex lens model.